Tradespace Exploration of Geometry for a Spacesuit Hip Bearing Assembly

Patrick McKeen
Department of Aeronautics and Astronautics
Massachusetts Institute of Technology
77 Massachusetts Avenue
Cambridge, MA 02139
pmckeen@mit.edu

Leia Stirling
Department of Industrial and Operations Engineering
University of Michigan
Ann Arbor, MI 48109
leias@umich.edu

***Abstract*—Space suits are crucial to human spaceflight, but can restrict motion, require additional energy, and increase injury risk. Previous planetary suits were largely based on flexible components, which generate additional forces on the occupant as they resist volumetric changes from flexing components. The NASA Mark III suit addresses this problem using a Hip Brief Assembly (HBA), composed of rigid, constant-volume sections connected by bearings. However, due to the rigid components and fixed degrees of freedom (DoFs), the HBA and other hard-component joint assemblies (HCJAs) have stricter bounds on motion. For example, previous analysis shows that the hip multi-DoF range of motion (ROM) for an HBA occupant is not well-aligned with the nominal hip ROM during gait (gait NHROM).**

In this paper, a set of methods for describing HCJA geometry and the effect on occupant ROM is presented. A generalized model builds on Denavit-Hartenberg parameterization to describe HCJA structure, rotation, and surface shape. Also included is a computational approach to estimate the multi-DoF ROM for joints of an HCJA occupant, and compare and score the suit-restricted ROMs against nominal, unencumbered ROMs.

These models are utilized to analyze HBA geometry and improve alignment between in-suit occupant ROM and gait NHROM. A set of design constraints based on feasible geometries and parameter bounds were devised and used to limit a tradespace analysis of alternate geometries in the HBA model. The geometries were evaluated and given a ROM score based on occupant access to gait NHROM. Over 1.3 billion alternate geometries were tested, with 100 million used to sample the tradespace. Of these designs, 52,276 met or bested the nominal geometry. The top-scoring geometry showed a more than sixfold improvement on access to gait NHROM, as well as a more natural neutral leg position, a significant increase in adduction range, and improved kneeling ability. The geometry also performed well across different anthropometries. The tradespace data set was used to analyze trends in HBA geometry, suggesting the most dominant factors behind a high ROM score is the cant angle in the Proximal and Distal sections.

TABLE OF CONTENTS

1. INTRODUCTION 1
2. HCJA MODEL 2
3. HBA DESIGN CONSTRAINTS 3
4. HCJA ROM MEASUREMENT AND COMPARISON 3
5. HBA TRADESPACE EXPLORATION 8
6. ANTHROPOMETRIC ANALYSIS 12
7. LIMITATIONS AND FUTURE WORK 14
8. SUMMARY 14
ACKNOWLEDGMENTS 15
REFERENCES 15
BIOGRAPHY 16

978-1-7281-2734-7/20/$31.00 ©2020 IEEE

1. INTRODUCTION

Extravehicular activity (EVA) space suits ("space suits" or "suits") have been used from the beginning of human spaceflight through the modern day. Many of these suits, including the currently-used EVA Mobility Unit (EMU) and Orlan suits, as well as the A7L, the original Apollo space suit, use flexible materials for the limbs [1]. While flexible limbs can allow for a great deal of motion, they can cause a problem with "springback" forces, where the limbs resist motion due to volumetric changes when the occupant moves [2, 3]. These springback forces can cause a variety of issues, including reduced mobility and increased energy usage for the suit occupant [4].

These issues can particularly impact lower limb movements; Apollo astronauts reported not only great difficulty with locomotion, but exertion in their thighs to the point of fatigue [5, 6]. Such extensive use of the thigh was likely connected to motions of the hip used for walking, indicating the suit hip joint and the gait motion may be particularly susceptible to springback forces [7, 8].

One alternative to avoid springback forces is hard-component joint assemblies (HCJAs), where the suit's degrees of freedom are captured by constant-volume rigid components connected by bearings [9, 10]. One example of such a hard-joint suit is the NASA demonstrator Mark III suit, which uses a hard-component Hip Bearing Assembly (HBA), shown in Figure 1, at the hips to allow for more mobility and mitigate springback forces [10]. However, the HBA (and other HCJAs) are susceptible to other mobility issues and can restrict the occupant's mobility [11, 12]. Movement within a hard-joint suit is bounded by the geometry and placement of the bearings [10]. If these bounds are misaligned with the occupant's natural motions, they are forced to use "programmed" motions [13, 14]. Programmed motions, which can be new and unnatural to the occupant, could increase injury risk, discomfort, and energy expenditure [14]. For example, motions with increased circumduction (like many space suits), have been shown to increase metabolic cost [15]. Addressing these issues, particularly by improving mobility, could reduce injury risk, discomfort, and energy expenditure for the astronauts [14, 16].

While the Mark III has much greater mobility than space suits with flexible limbs, it still forces the users into programmed motions [17]. In particular, previous research has shown that the motion envelope of the Mark III occupant's hips is misaligned with the hip positions usually used for gait [12].

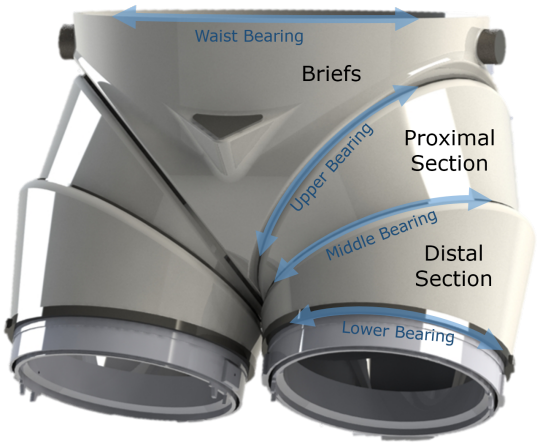


Figure 1: **Rendering of Mark III HBA, with components and bearings labeled.**

As a result, occupants of the Mark III are forced to use programmed motions for ambulation [13, 17].

This paper presents new procedures to model HCJAs and to estimate and quantify their impact on the occupant's range of motion (ROM). Specifically, a model based on Denavit-Hartenberg parameters is introduced to describe HCJA geometry (Section 2), a process to approximate ROM based on this geometry is demonstrated (Section 4), and a methodology based on spherical projects is shown to permit quantitative comparison across multiple dimensions of an ROM in an integrated manner (Section 4). These methods are used to explore possible alternate HBA geometries in a tradespace analysis. The generalized parameterization and model of HCJAs is discussed in Section 2, and applied to the HBA. The limits on possible variations of the HBA geometry, bounding the design space, are determined in Section 3. A method for scoring the mobility of an HCJA's occupant based on their ROMs is detailed in Section 4. Section 5 combines the model, bounds, and scoring method into a tradespace exploration of the HBA and discusses those results. The validity of the results for different anthropometries is tested and discussed in Section 6. Section 7 suggests possible extensions, while Section 8 provides a summary.

2. HCJA Model

To model HCJAs, several simplifications were made:

- Every HCJA is a simple rigid body tree.
- The HCJA does not include the final component on any limb (there is always a glove, boot, or other component that is not part of the HCJA).
- Soft-good components are excluded.
- Motion in the HCJA is ideal, without flexing or bending. All rotation is around the defined axes.
- Every component edge is a circle in $\mathbb{R}^3$.
- There is no overlap between components.
- Components (excluding bearings[1]) are infinitely thin surfaces in $\mathbb{R}^3$.

[1]Bearings are three-dimensional flat rings with constant heights. They are not parameterized separately, but have internal and external radii matching the radii of the edges to which they are adjacent.

With these simplifications, the shape and structure of the HCJAs can be described in six parameters per section (d, θ, α, a, r_t, and r_b) plus an additional parameter (h) per joint. To define the components, the circles which serve as their edges must be described. We note that that the circles must lie on a plane normal to the axis of rotation of each component. The position along this axis and the radii of the circle then fully describe the edges. The axes of rotation of the HCJA are described in coordinate frames using Denavit-Hartenberg (DH) parameters. This parameterization, which involves specifically defining the coordinate frame axes and origins, allows for the transformation between the coordinate frames (including the respective axes of rotation) for each component to be described in four parameters: θ, a, d, and α. Subscripts identify the component to which the parameters belong. For example, for transforming from frame m to the subsequent frame n, the parameters are θ_m, a_m, d_m, and α_m. Using four-dimensional homogeneous coordinates, the transformation from one frame to another, in this case the transformation of a point in frame n to the same point in m, ${}^mT_n$, is

$$ {}^mT_n = \begin{bmatrix} \cos\theta_m & -\sin\theta_m\cos\alpha_m & \sin\theta_m\sin\alpha_m & a_m\cos\theta_m \\ \sin\theta_m & \cos\theta_m\cos\alpha_m & -\cos\theta_m\sin\alpha_m & a_m\sin\theta_m \\ 0 & \sin\alpha_m & \cos\alpha_m & d_m \\ 0 & 0 & 0 & 1 \end{bmatrix}. \quad (1) $$

In this application, θ are treated as constant and rotation about the bearings (putting the HCJA in a new "pose") is shown by shifting the value of θ by ϕ, where ϕ is the angle of rotation of the bearing. Including this representation in Eq. (1) makes the transformation between frames

$$ \begin{bmatrix} \cos(\theta_m+\phi_m) & -\sin(\theta_m+\phi_m)\cos\alpha_m & \sin(\theta_m+\phi_m)\sin\alpha_m & a_m\cos(\theta_m+\phi_m) \\ \sin(\theta_m+\phi_m) & \cos(\theta_m+\phi_m)\cos\alpha_m & -\cos(\theta_m+\phi_m)\sin\alpha_m & a_m\sin(\theta_m+\phi_m) \\ 0 & \sin\alpha_m & \cos\alpha_m & d_m \\ 0 & 0 & 0 & 1 \end{bmatrix}. \quad (2) $$

or, separating ϕ into a rotation matrix,

$$ {}^{J(\phi_m)}{}^mT_n = \begin{bmatrix} \cos\phi_n & -\sin\phi_n & 0 & 0 \\ \sin\phi_n & \cos\phi_n & 0 & 0 \\ 0 & 0 & 1 & 0 \\ 0 & 0 & 0 & 1 \end{bmatrix} \begin{bmatrix} \cos\theta_m & -\sin\theta_m\cos\alpha_m & \sin\theta_m\sin\alpha_m & a_m\cos\theta_m \\ \sin\theta_m & \cos\theta_m\cos\alpha_m & -\cos\theta_m\sin\alpha_m & a_m\sin\theta_m \\ 0 & \sin\alpha_m & \cos\alpha_m & d_m \\ 0 & 0 & 0 & 1 \end{bmatrix}. \quad (3) $$

Examples of the DH parameters can be seen in Figure 2, showing the HBA with these parameters labeled.

As shown in the example in Figure 2, the coordinate frame origins do not necessarily align with the physical joints of the suit. The z-axis of the coordinate frame ($\hat{z}_m$ for frame m, defined similarly for $\hat{x}$ and $\hat{y}$) runs through the center of each corresponding physical joint. The location of the component edges can be specified by describing a position along this axis. Components of the HCJA do not have an overlap in this model, so the edges of the two adjacent components lie in the same plane normal to this axis. The position of this plane is specified with an $h_{m/n}$ parameter, where m and n indicate the indices of the two components meeting at that joint. Examples of the h parameters can be seen in Figure 2.

As edges are assumed to be circles centered around the z-axis, they can be defined by the radii (r_{mt} and r_{mb}, corresponding to the top and bottom edges). For component m with component n distal to it and component l proximal to it, the top edge can be given by

$$ {}^m\vec{t}_m(p) = \begin{bmatrix} r_{mt}\cos p \\ r_{mt}\sin p \\ h_{l/m} \\ 1 \end{bmatrix} \quad (4) $$

and the bottom edge by

$$ {}^{m}\vec{b}_m(p) = {}^{m}T_n \begin{bmatrix} r_{mb}\cos p \\ r_{mb}\sin p \\ h_{m/n} \\ 1 \end{bmatrix} \tag{5} $$

In both Eqs. (4) and (5), p is a parametric variable describing the functions of the edges. It does not have a defined value or significance between the equations. The pre-appended superscript in the expressions indicates the coordinate frame in which the vectors are being expressed. For example, if $\vec{b}_m$ was instead described in frame n (note that $\vec{b}_m$ is coplanar with $\vec{t}_n$), it would be

$$ {}^{n}\vec{b}_m(p) = \begin{bmatrix} r_{mb}\cos p \\ r_{mb}\sin p \\ h_{m/n} \\ 1 \end{bmatrix} \tag{6} $$

These equations and parameters fully describe the edges and movement of each component of the HBA. Surfaces between the edges can be generated to represent the physical shapes of the components. (For more detailed implementation of surfaces, see [18].)

Unlike the other parts, bearings are not treated as flat surfaces. Instead, they are defined as flat rings with a height of $l_{m/n}$, where m and n are the components to which the bearing is adjacent. The bearing has internal and external radii equal to the radii of the edges of components m and n to which it connects. The bearing's top edge is coplanar with the joint ($h_{m/n}$ along $\hat{z}_m$ from the origin of frame m), so the bottom edge is $l_{m/n}$ further along $\hat{z}_m$.

3. HBA DESIGN CONSTRAINTS

The geometry model described in Section 2 was applied to the HBA, yielding the values listed in Table 1. By modifying the values of these parameters, different HBA geometries can be achieved. However, to explore this question efficiently, constraints are needed to ensure feasible geometry. For the HBA, constraints were created for the Briefs and for the Proximal and Distal Sections. These constraints can be found in Tables 2 and 3, respectively. Some of these constraints contain limits. These limits were sourced from the current HBA geometry or were created to allow for a wide range of possibilities, subject to reasonable limits.

Beyond these geometric constraints, parameter bounds were determined to define and limit the design space of HBA geometries. These bounds, summarized in Table 1, were chosen in an attempt to balance computational feasibility of the space, a large design space, and physical reasoning. Both these bounds and the constraints above were used in the tradespace exploration in Section 5.

4. HCJA ROM MEASUREMENT AND COMPARISON

A generalized method to score different HCJAs was devised, and applied to measure and compare different HBA geometries within the bounds in Section 3. This scoring method treats the Suited and Unsuited multi-dimensional ROMs of the occupant's relevant joint as regions on the surface of the unit sphere. The area of the overlap of these regions (maximally, equal to the Unsuited ROM) is a proxy for how severely that joint is restricted by the suit. This section will describe estimating these regions for Unsuited and Suited ROMs using unit vectors in $\mathbb{R}^3$ (these correspond to points on the unit sphere surface). The procedure for comparing these unit-vector-defined regions to generate the ROM score is also detailed, as well as the application of these methods to the HBA.

Table 1: Table of bounds on HBA parameters, with units and nominal value.

Parameter	Units	Nominal	Min	Max
$h_{0/1}$	m	0	0[d]	0[d]
r_{1t}	m	0.232	0.232[d]	0.232[d]
a_1	m	0.032	-0.125[a]	0.125[a]
d_1	m	-0.106	-0.2[e]	0[b]
θ_1	rad	2.793	$\frac{\pi}{2}$[c]	$\frac{3\pi}{2}$[c]
α_1	rad	-0.908	$-\frac{5\pi}{8}$[a]	$\frac{5\pi}{8}$[a]
$h_{1/2}$	m	-0.128	-0.25[e]	0[b]
r_{1b}	m	0.134	0.134[d]	0.134[d]
r_{2t}	m	0.158	0.158[d]	0.158[d]
a_2	m	0.005	-0.1[e]	0.1[e]
d_2	m	-0.103	-0.2[e]	0[b]
θ_2	rad	π	π[d]	π[d]
α_2	rad	-0.398	$-\frac{\pi}{2}$[a]	$\frac{\pi}{2}$[a]
$h_{2/3}$	m	-0.087	-0.25[e]	0[b]
r_{2b}	m	0.128	0.128[d]	0.128[d]
r_{3t}	m	0.140	0.140[d]	0.140[d]
a_3	m	0	-0.1[e]	0.1[e]
d_3	m	-0.090	-0.2[e]	0[b]
θ_3	rad	0	0[d]	0[d]
α_3	rad	-0.404	$-\frac{\pi}{2}$[a]	$\frac{\pi}{2}$[a]
$h_{3/4}$	m	-0.1	-0.25	0[b]
r_{3b}	m	0.114	0.114[d]	0.114[d]

[a] This bound is outside the limits on the parameter established by geometric constraints and thus does not prevent consideration of any viable geometries.
[b] This bound ensures proper structure.
[c] This bound limits the exploration space to improve computation time, but all possible geometries are preserved.
[d] The parameter of this bound was held constant in tradespace exploration, so the lower and upper bounds were the same.
[e] This bound was selected to give a large exploration space that is still tractable.

Unsuited ROM

The Unsuited ROM is the control for the comparison method described later in this section. It is the nominal ROM for the occupant's joint corresponding to the HCJA, when unsuited and unencumbered. The Unsuited ROM of the joint can be calculated either for specific tasks (such as the ROM of the hip used during gait, the ROM of the knee used in kneeling, the ROM of the wrist used in sample collection, or similar definitions) or for the joint's entire possible motion envelope (the full range angles of the shoulder, hip, wrist, or other joint usable when unsuited). In either case, the ROM bounds must be described as unit vectors.

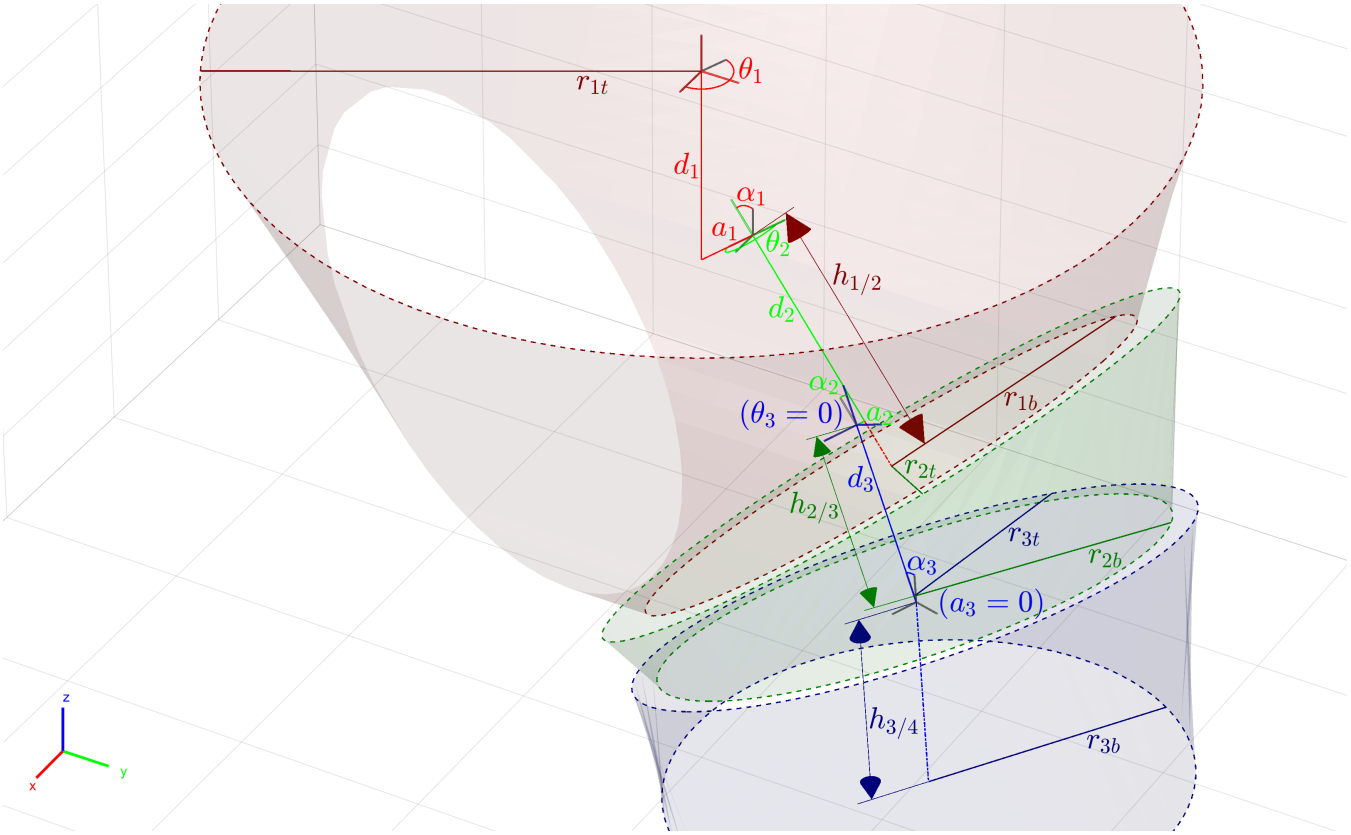


Figure 2: **Mark III HBA with model parameters and edges labeled.**

Table 2: **Table of geometric constraints on HBA Briefs.**

Constraint	Motivation	Formula
Direction	For comfort and utility, leg should point forward, outward, and down.	$\left({}^1T_2 \begin{bmatrix} 0 \\ 0 \\ -1 \\ 0 \end{bmatrix} \right) \cdot \begin{bmatrix} 1 \\ 0 \\ 0 \\ 0 \end{bmatrix} \geq 0, \left({}^1T_2 \begin{bmatrix} 0 \\ 0 \\ -1 \\ 0 \end{bmatrix} \right) \cdot \begin{bmatrix} 0 \\ 1 \\ 0 \\ 0 \end{bmatrix} \geq 0, \left({}^1T_2 \begin{bmatrix} 0 \\ 0 \\ -1 \\ 0 \end{bmatrix} \right) \cdot \begin{bmatrix} 0 \\ 0 \\ 1 \\ 0 \end{bmatrix} \leq 0$
Height	Leg hole bearings must not be too near top edge, and Briefs must not be too tall.	$\forall p \in [0, 2\pi)\,,\ -0.3\text{ m} \leq \left({}^1\vec{b}_1(p) \cdot \begin{bmatrix} 0 \\ 0 \\ 1 \\ 0 \end{bmatrix} \right) \leq -0.03\text{ m}$
Gap	Leg hole bearings must not be too close to each other.	$\forall p \in [0, 2\pi)\,, \left({}^1\vec{b}_1(p) \cdot \begin{bmatrix} 0 \\ 1 \\ 0 \\ 0 \end{bmatrix} \right) \geq \frac{0.03\text{ m}}{2}$
Width	To avoid forcing abduction, leg holes must fall within the circle of the top edge.	$\forall p \in [0, 2\pi)\,, \left\| \left({}^1\vec{b}_1(p) \right)_{1:3} \times \begin{bmatrix} 0 \\ 0 \\ 1 \end{bmatrix} \right\| \leq r_{1t}$

The exact method of conversion to unit vectors depends on the manner in which the ROM is initially described. For example, if the ROM is initially described as a set of positions in $\mathbb{R}^3$ that the relevant limb can adopt, this representation is equivalent to the unit vectors necessary for comparison (though normalization may be required). However, most data will likely be in less convenient formats. One common method of describing ROM in literature, which will serve as our example, is a pair of angular ranges indicating the maximum and minimum angles for the human joint in two different degrees of freedom (DoFs) [7, 19]. This representation can also be applied to a three-DoF joint, like the human hip, if one of the DoFs is neglected. For the HBA analysis in this paper, internal and external rotation–rotating the knee and foot without moving the thigh–was ignored, instead considering just the position of the knee relative to the hip. A unit vector (representing the relevant limb) can be rotated by these angular bounds to create the unit vectors defining the boundaries of the Unsuited ROM. In this case, we will convert hip position angular ranges for nominal gait to an Unsuited ROM.

Table 3: **Table of geometric constraints on HBA Proximal and Distal Sections. The expressions hold for $n \in \{2, 3\}$.**

Constraint	Motivation	Formula
Length	Long components will limit movement and worsen fit.	$\left\| \begin{bmatrix} 0 \\ 0 \\ h_{n-1/n} \\ 1 \end{bmatrix} - {}^{n}T_{n+1} \begin{bmatrix} 0 \\ 0 \\ h_{n/n+1} \\ 1 \end{bmatrix} \right\| \leq 0.15 \text{ m}$
Angle	Occupant's thigh will not fit if there is too sharp an angle between planes of top and bottom edges.	$\begin{bmatrix} 0 \\ 0 \\ 1 \\ 0 \end{bmatrix} \cdot \left({}^{n}T_{n+1} \begin{bmatrix} 0 \\ 0 \\ 1 \\ 0 \end{bmatrix} \right) \geq \cos\left(60^\circ\right)$
Skew	If top and bottom edges are too far apart compared to their planes (too skewed), the occupant's limb will not fit through.	$\left\| \begin{bmatrix} 0 \\ 0 \\ 1 \end{bmatrix} \times \left({}^{n}T_{n+1} \begin{bmatrix} 0 \\ 0 \\ h_{n/n+1} \\ 1 \end{bmatrix} \right)_{1:3} \right\| \leq r_{nt}, \left\| \begin{bmatrix} 0 \\ 0 \\ 1 \end{bmatrix} \times \left({}^{n+1}T_{n} \begin{bmatrix} 0 \\ 0 \\ h_{n-1/n} \\ 1 \end{bmatrix} \right)_{1:3} \right\| \leq r_{nb}$
Height	If the top and bottom edges overlap one another's planes, fit will be impossible.	$\forall p \in [0, 2\pi), \left(\begin{bmatrix} 0 \\ 0 \\ 1 \\ 0 \end{bmatrix} \cdot {}^{n}\vec{b}_n(p) \right) \leq h_{n-1/n}$
Gap	Edges cannot be too close to one another, to allow space for bearings and structure.	$\forall p_t [0, 2\pi), \forall p_b \in [0, 2\pi), \left\| {}^{n}\vec{t}_n(p_t) - {}^{n}\vec{b}_n(p_b) \right\| \geq l_{\min}$

Table 4: **Extreme hip angles for human gait (in $^\circ$). Signs added to indicate direction.**

	Direction	Maximum	Converted
ψ_{flex}	Flexion	40	-40
ψ_{ext}	Extension	10	10
ψ_{ab}	Abduction	5	5
ψ_{ad}	Adduction	10	-10

The values for angular bounds of hip position during gait, shown in Table 4, were sourced from the Clinical Gait Analysis Normative Gait Database [20]. The resting limb (the thigh, in this case) is represented by a unit vector in the $-\hat{z}$ direction. This vector is rotated about the $\hat{x}$-axis by the ab/adduction bound angles, then rotated about the (original) $\hat{y}$-axis by the flexion/extension bound angles, to give the unit vectors representing the four "corners" of the Unsuited ROM. (This approach differs from the standard established by the International Society of Biomechanics (ISB), where rotation is intrinsic instead of extrinsic and flexion/extension is applied before ab/adduction [21].) These corner unit vectors are as follows:

$$\begin{bmatrix} -\sin\psi_{\text{ext}}\cos\psi_{\text{ad}} \\ \sin\psi_{\text{ad}} \\ -\cos\psi_{\text{ext}}\cos\psi_{\text{ad}} \end{bmatrix}, \begin{bmatrix} -\sin\psi_{\text{flex}}\cos\psi_{\text{ad}} \\ \sin\psi_{\text{ad}} \\ -\cos\psi_{\text{flex}}\cos\psi_{\text{ad}} \end{bmatrix}, \tag{7}$$

$$\begin{bmatrix} -\sin\psi_{\text{flex}}\cos\psi_{\text{ab}} \\ \sin\psi_{\text{ab}} \\ -\cos\psi_{\text{flex}}\cos\psi_{\text{ab}} \end{bmatrix}, \text{ and } \begin{bmatrix} -\sin\psi_{\text{ext}}\cos\psi_{\text{ab}} \\ \sin\psi_{\text{ab}} \\ -\cos\psi_{\text{ext}}\cos\psi_{\text{ab}} \end{bmatrix}. \tag{8}$$

Suited ROM

The Suited ROM is the envelope of the motions available to the occupant when limited by the HCJA. Unlike its Unsuited counterpart, the Suited ROM always describes the total motion envelope available to the occupant's joint. The total ROM is used for Suited ROM even with task-based definitions of Unsuited ROM. This approach prevents the occupant's experience or strategy from influencing the estimated Suited ROM.

The Suited ROM could be based on experimental data or gathered from literature, but that may not be feasible for a tradespace analysis, rapidly iterated design process, or similar endeavor. Instead, a general approach to estimating the Suited ROM for an HCJA with arbitrary geometry was developed. The estimation is approached by simulating the occupant's limb inside the suit across the space of possible poses, and testing for intersection between the limb and suit.

The limb is critical to this estimation, as it allows the discounting of HCJA poses where the occupant's body would intersect the HCJA. The simulated limb models the body part immediately distal to the relevant human joint (e.g., for the HBA, we consider the thigh). For every HCJA pose, the limb has two properties necessary to estimate the Suited ROM: a set of line segments indicating the limb's shape and a pair of points indicating the limb's orientation (a base point and a tip point, both in the global frame). For a given limb, the positions of these points and lines must be entirely and uniquely specified by the HCJA pose. The vector between the base and tip points in each pose is used to describe the orientation of the limb (and thus the position of the human's joint) to estimate the Suited ROM. The line segments representing the limb surface are used to test for intersection between the leg and the HCJA.

For example, in the HBA, the simulated limb was the thigh, with a base point at the hip and a tip point at the knee. As shown in Figure 3, the base point was the upper bearing centroid and the tip point was a constant position[2] in the Distal Section frame. The same figure shows how the thigh was approximated with eight line segments spaced evenly around a truncated cone. The cone's axis runs between the

[2]The position can be described as ${}^{3}T_{4}\,[0\text{ m} \quad 0\text{ m} \quad -0.376\text{ m}]^{T}$ and was based on the nominal Mark III HBA geometry.

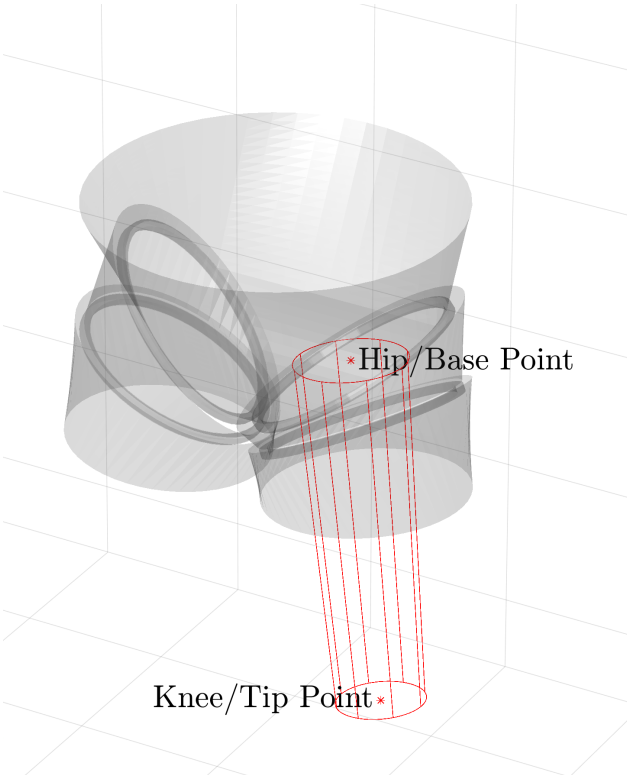


Figure 3: **Mark III HBA with simulated thigh.**

Table 5: **Dimensions of simulated thigh used in HBA ROM analysis.**

Dimension	Value (cm)	ANSUR # or Equation
Thigh Circumference	62.40	#78
Knee Circumference	40.80	#60
Thigh Radius	6.95	$\frac{0.7}{2\pi}$ (Thigh Circumference)
Knee Radius	5.52	$\frac{0.85}{2\pi}$ (Knee Circumference)

hip and knee points, with circles at each end centered on and normal to the axis. The radii of the circles, shown in Table 5, were calculated from values[3] in the 2012 Anthropometric Survey of U.S. Army Personnel (ANSUR II) [22].

Using the simulated limb, the Suited ROM is estimated by considering the space of possible HCJA poses and noting the positions where the limb and HCJA do not intersect. The space of possible poses is a set of N_{DoF} angular ranges between 0 and 2π, where N_{DoF} is the number of DoFs or bearings in the HCJA. Each of these ranges indicates the angular displacement of a bearing, but testing the full range of each bearing is unnecessary and increases computational complexity. The angles considered for each DoF can be limited based on the feasibility of possible motions of the suit's occupant and the purpose of the ROM measurement. For example, when testing an ROM score, only the overlap matters, bearing positions which would only generate Suited ROM points far from the Unsuited ROM can be discounted. The N_{DoF} angular ranges can thus be limited and then sampled for computational simplicity. For each joint n, there will be an upper and lower bound on this range, $\phi_{n,\text{min}}$ and $\phi_{n,\text{max}}$, and the angles sampled will be separated by increment $\Delta\phi_n$. The Suited ROM is estimated using poses created from these sampled angles, testing every combination of one from each set of sampled angles (the total number of poses is the product of the cardinalities of the sets).

For each of these tested poses, the limb is simulated and its line segments are tested for intersection with the surfaces of the HCJA (sourced from a .STL file or the model in Section 2). If there is no intersection, the orientation of the simulated limb in this pose is considered to be within the Suited ROM and the vector corresponding to the limb's orientation (expressed in the global frame) is recorded. This process is repeated for each HCJA pose sampled from the space of possible poses. The set of non-intersecting vectors recorded across the space of possible poses are normalized to unity. These unit vectors correspond to points on the surface of the unit sphere, which provide samples of points inside the Suited ROM. This set of points can be converted to a specific shape on the unit sphere surface using a slight variation on the ROM scoring process below. However, for ROM comparison, the shape does not need to be calculated–only these points/vectors from sampled poses are required.

Suited vs Unsuited ROM Comparison

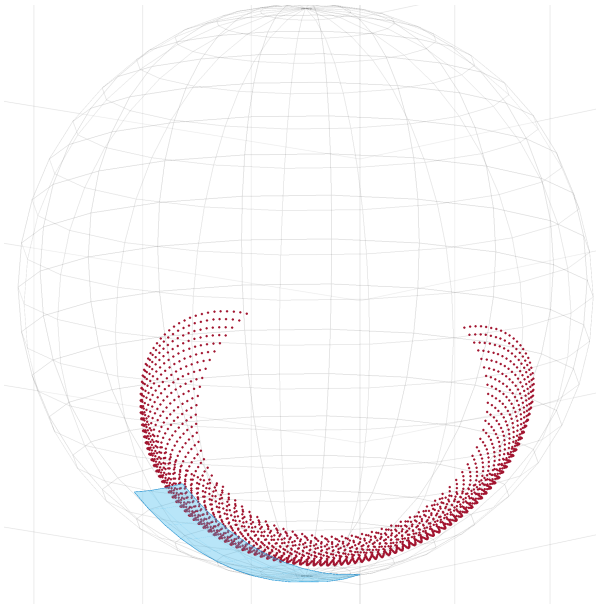
To assess the impact of an HCJA on the occupant's multi-DoF (MDoF) ROM, the Unsuited and ROM can be compared. The Unsuited ROM should be in the form of a set of unit vectors that define a shape on the unit sphere surface, corresponding to the limits of the relevant human joint's ROM when unencumbered. The Suited ROM is also represented by a collection of unit vectors, which are samples of feasible occupant limb positions of the occupant when wearing the HCJA. These ROMs can be compared by converting the scattered points of the Suited ROM into a bounded shape, and comparing this shape to the Unsuited ROM. A quantifiable metric termed the "ROM score" is defined. The ROM score is proportional to area of the overlap between the Unsuited and Suited ROM shapes. When there is no overlap, the score is zero. The maximum ROM score is the original Unsuited ROM area, presented as a value normalized to the surface area of the unit sphere. We begin with the unit vectors of the Suited and Unsuited ROMs, illustrated in Figure 4a. The procedure is as follows:

1. **Rotate Suited and Unsuited ROM Vectors:** To avoid geometric distortion, the Suited and Unsuited ROM vectors must be rotated away from spherical coordinate singularities (the "poles" or $\pm z$-axes). Any rotation (or set of perpendicular rotations) that moves the overlap area (or, ideally, all of both ROMs) so that it does not cross a pole will work, as long as it is consistently applied to both the Suited and Unsuited ROMs. The process here demonstrates a method used for the HBA with an Unsuited ROM simply defined as angular bounds on two DoFs, but similar approaches can be used to find the rotation bounds for any Unsuited ROM.

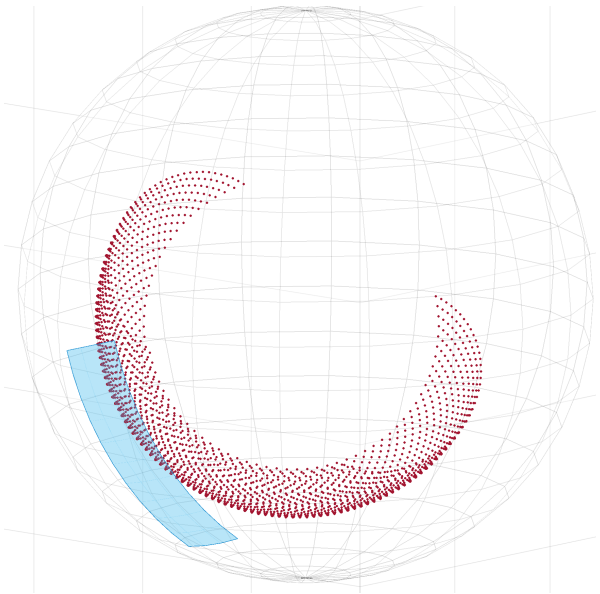
We must find a rotation, which we will define to be angle ρ around the y-axis in the negative direction, that moves the Suited and Unsuited ROM vectors away from the $-z$ singularity, but is not so large as to make the ROMs intersect the $+z$ singularity. The Unsuited ROM for the HBA spans angles[4] from $-\psi_{\text{flex}}$ to ψ_{ext} around the positive y-axis, so the rotation ρ must fall between $-\psi_{\text{ext}}$ and $\pi + \psi_{\text{flex}}$.

[3] 50th percentile male values used. Radii converted from circumference using $\frac{1}{2\pi}$, with a scaling factor to account for compression of soft tissue.

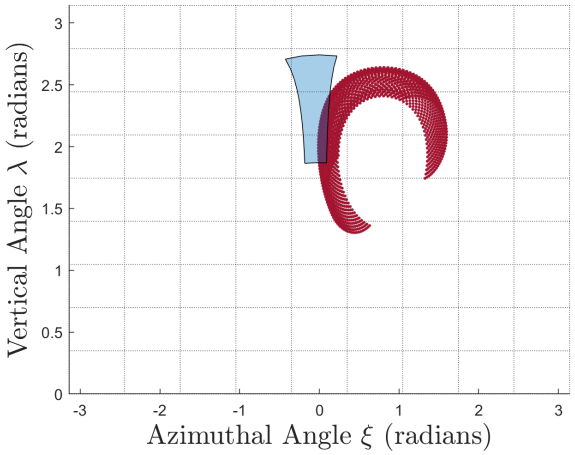
[4] This assumes all vectors point towards points in the lower unit hemisphere. If that is not the case, this approach still works, but x_{min} and x_{max} are no longer the values to use. The value of the angles more than 90 degrees must be considered.



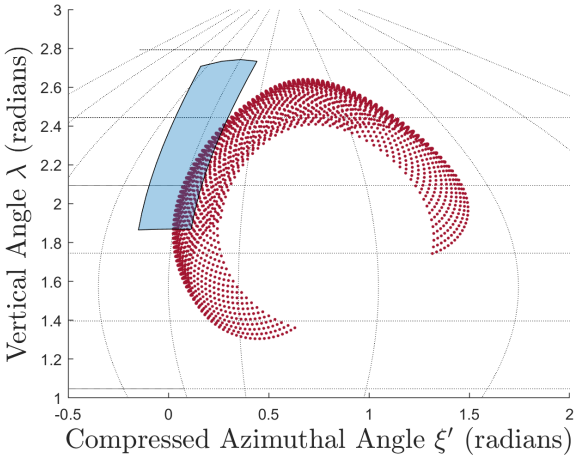
(a) Unsuited ROM region (blue) and Suited ROM points (red) on unit sphere.



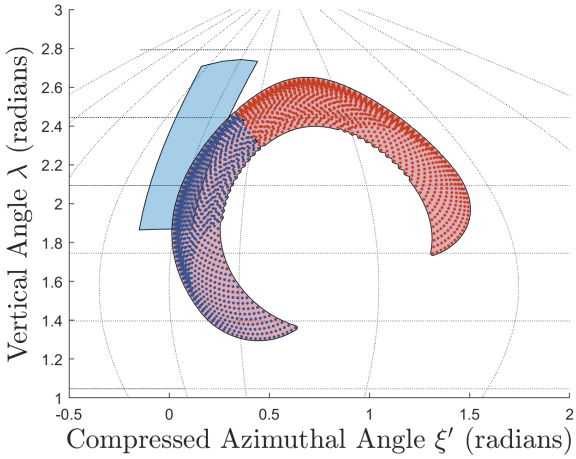
(b) Unit sphere ROM rotated away from singularities at the poles.



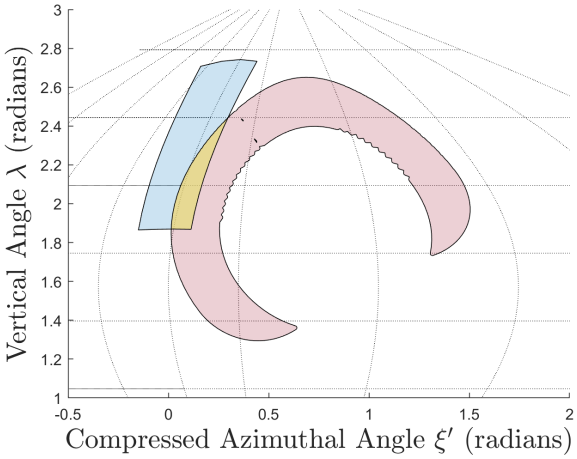
(c) ROM mapped from unit sphere to spherical coordinates.



(d) Spherical coordinate ROM proportions corrected using equal-area sinusoidal projection.



(e) Shapes for area calculation generated from Suited ROM points. (Point colors indicate clusterings.)



(f) Unsuited and Suited ROM shapes, with overlap in yellow. (Score is area of overlap.)

Figure 4: **Steps to calculate ROM score.**

The equivalent angular bounds for the Suited ROM must be generated from the data. We discount Suited ROM vectors with significant y-coordinates, as no ρ value will bring them near the poles. We instead consider vectors with y-coordinates that satisfy $\sin\psi_{\text{ab}} \geq y \geq \sin\psi_{\text{ad}}$. (If there are no such vectors, there is no overlap. The ROM score is 0.) We can say these vectors span an angular range of $\arcsin x_{\text{min}}$ to $-\arcsin x_{\text{max}}$ from the $-z$ singularity, where the x variables are the least and greatest x-coordinates in the subset. The rotation ρ must therefore be between $-\arcsin x_{\text{min}}$ and $\pi - \arcsin x_{\text{max}}$.

The value of ρ must fall within the rotational bounds established for both the Suited and Unsuited vectors, so we have

$$\rho > \rho_{\text{min}} = \max\left(-\arcsin\left(x_{\text{min}}\right), -\psi_{\text{ext}}\right) \tag{9}$$

and

$$\rho < \rho_{\text{max}} = \min\left(\pi - \arcsin\left(x_{\text{max}}\right), \pi + \psi_{\text{flex}}\right). \tag{10}$$

A value must then be selected between these bounds. The suggested value is 20% of the range away from ρ_{min}, to minimize rotation but be sufficiently far from the bounds. In other words, $\rho = \rho_{\text{min}} + 0.2\left(\rho_{\text{max}} - \rho_{\text{min}}\right)$. The selection of the rotation is shown in Figure 5. Every vector in the Suited or Unsuited ROM is rotated by ρ around the negative y-axis (or $-\rho$ about the positive y-axis). Examples of these rotated vectors can be seen in Figure 4b.

2. **Convert to Spherical Coordinates:** The now-rotated vectors of the Suited and Unsuited ROM are converted to spherical coordinates. As θ and ϕ are already used in this text, we will use a convention where λ is inclination (measured from the xy-plane), ξ is azimuth, and r is length. (All vectors under consideration are normalized, so length r is ignored.) For a given unit vector $\hat{v} = \begin{bmatrix} x & y & z \end{bmatrix}^T$, conversion follows according to

$$r = \sqrt{x^2 + y^2 + z^2}, \tag{11}$$

$$\lambda = \arccos\frac{z}{r} = \arccos z, \tag{12}$$

and

$$\xi = \text{atan2}(y, x). \tag{13}$$

To ensure there is no issue with the discontinuity from atan2, the range of ξ can be adjusted based on the position and shape of the ROMs. For example, it could be adjusted to go from $-\frac{\pi}{2}$ to $\frac{3\pi}{2}$ by incrementing all values of $\xi \leq -\frac{\pi}{2}$ by 2π. With the length constant, the vectors are now expressed as points in two dimensions, as shown in Figure 4c.

3. **Sinusoidal Projection:** With the conversion to spherical coordinates, the regions on the sphere are now projected to a two-dimensional map to estimate the overlapping area. There are several projections that can be used (exactly like there are many map projections), with some variants causing distortions that we want to eliminate [23]. The approach used here to avoid distortion is similar to the sinusoidal projection, an area-preserving projection [24]. We scale the ξ component (offset from an arbitrary middle point) by the sine of the λ component. The middle point selected is the mean of all ξ values for all vectors in the Suited ROM, $\mu_{\xi,\text{suit}}$. All vectors in both ROMs retain the same relative position to each other, but move towards $\mu_{\xi,\text{suit}}$ near the "poles" of the spherical coordinate system. In other words, for every vector $u = (\xi, \lambda)$, there is a transformation to $u' = (\xi', \lambda)$ by the rule

$$\xi' = (\xi - \mu_{\xi,\text{suit}})\sin\lambda + \mu_{\xi,\text{suit}}. \tag{14}$$

A shape formed by parts which have undergone this transformation will have a Cartesian area proportional to the area of the original shape on the unit sphere surface. The effect of this projection can be seen in Figure 4d.

4. **Define Polyshapes for ROMs:** With ROM vectors rotated, transformed, and projected, the actual comparison can proceed. If there are 10 or fewer (this boundary was selected by trial-and-error) valid points in the Suited ROM, the code returns an area overlap of zero. Otherwise, it continues as described here.

Shapes were created using MATLAB's polyshape functionality. However, certain HCJA geometries produce unconnected areas of points within the ROM. To prevent the creation of inaccurate "bridge" areas, a cluster analysis was performed on the set of (ξ', λ)-encoded Suited ROM points, using MATLAB's evalclusters function. A k-means clustering algorithm with a silhouette clustering evaluation criterion was used. Clustering is attempted for a cluster number from 1 to 5, and the optimal number is found by the function, using the criteria established by MATLAB [25].

For each of the clusters identified (shown in Figure 4e), the points in the cluster are considered and an attempt is made to form a sub-shape. The boundary points of the cluster are found using the boundary function with a consistent "shrink factor" of 0.8. This value was found by trial-and-error to produce a tight-fitting edge that represented the shape well. If the boundary command returns a list of three or more points, a shape is created from these points using MATLAB's polyshape function. Otherwise, the sub-shape is discarded. To ensure good meshing with other sub-shapes (as the clustering algorithm does sometimes divide one large group into smaller groups), the shape is then "buffered," creating a rim around the shape. This is achieved with the polybuffer function, and the distance of buffering is set to the square root of the area of the shape (calculated using the area function), scaled by 0.02. The shape is then simplified using the polyshape simplify function, to remove duplicate vertices and crossing edges.

The process is applied to each cluster. Using the union function, the resulting shapes from each cluster are combined. If all clusters are tested, and no clusters have produced valid boundaries and shapes, all sub-shapes are non-valid and the ROM score is 0. A polyshape object is also calculated from the transformed vectors of the Unsuited ROM. The generated polyshapes can be seen in Figure 4e.

5. **Calculate Overlap Area:** The overlap between the polyshape objects representing the Suited and Unsuited ROMs is found using MATLAB's intersect function for polyshape objects. This returns a new polyshape object that is the intersection, or overlap, of the two ROMs, as shown in Figure 4f. The area of this overlap polyshape is found using the area function. This area indicates the Suited and Unsuited ROMs overlap. The overlap area, scaled by the surface area of the unit sphere, $\frac{1}{4\pi}$, is the ROM score.

5. HBA TRADESPACE EXPLORATION

By varying the parameters in Section 2 within the bounds described in Section 3, different alternatives to HBA geometry could be explored. These geometries were scored in terms of gait ROM using the methodology in Section 4. Even with the focus limited to the human hip ROM and the HBA geometry parameterized into a thirteen-dimensional space, the space of possible HBA geometries is complex to explore.

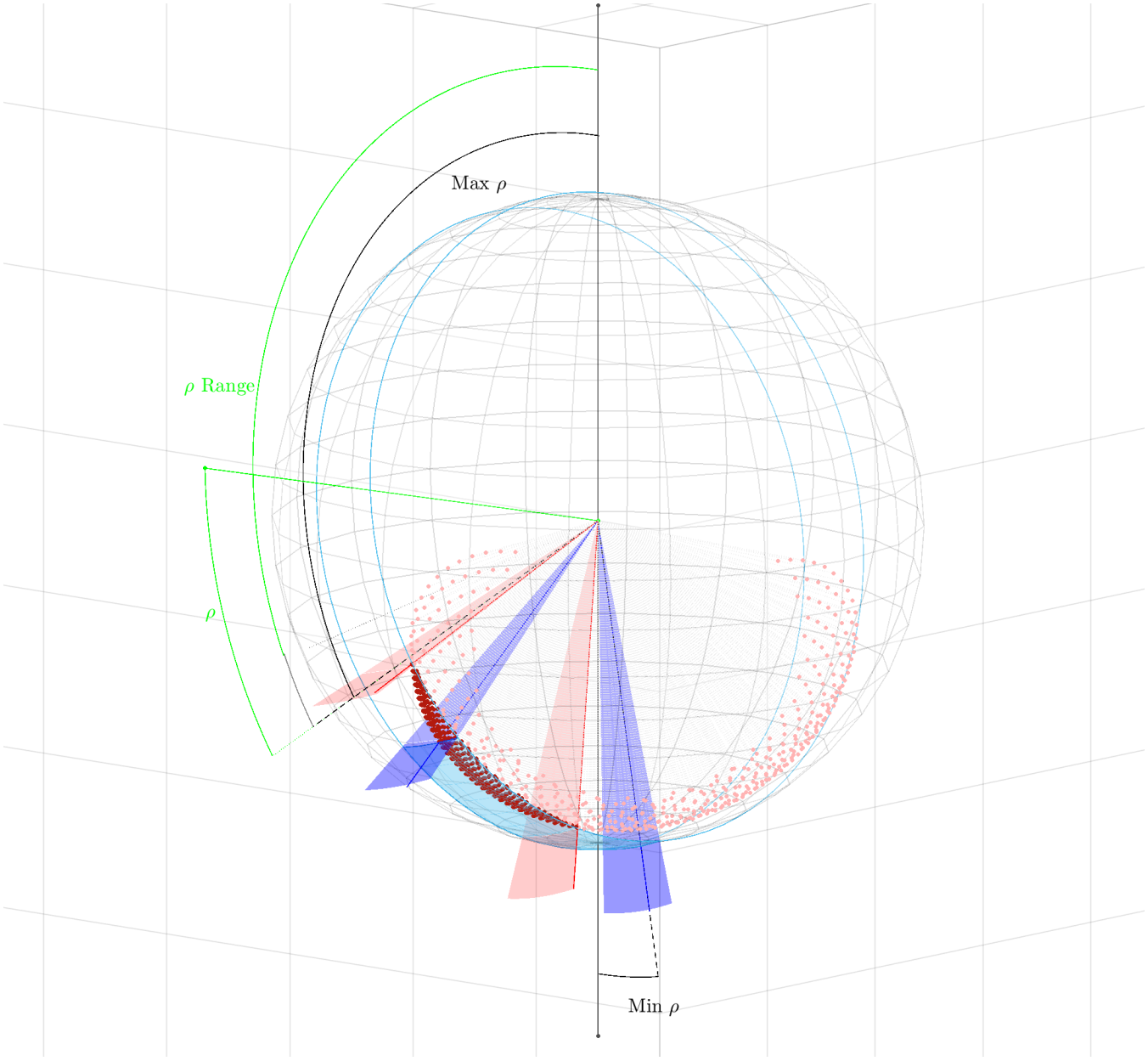


Figure 5: **Derivation of rotation ρ for separating ROM vectors from spherical coordinate singularities. Red and pink dots are points in the Suited ROM. Blue box is the Unsuited ROM. Red dots are points in the Suited ROM relevant to rotation, and red lines show maximum/minimum points in that group (those most limiting the overall rotation). Blue lines show maximum/minimum points for the Unsuited ROM. Black dotted lines show overall maximum/minimum points (from both ROMs), used to find rotation range (maximum/minimum values of ρ). Green arcs show rotation range and selected rotation, ρ.**

The impact of the parameters on the ROM score is highly nonlinear, with many local minima and maxima. These issues preclude an optimization approach. Instead, to explore the tradespace and understand how ROM score variations, the HBA geometry was sampled at a number of points and the ROM was analyzed for each.

Initial experiments indicated that the Briefs parameters ($h_{1/2}$, a_1, d_1, θ_1, and α_1) had little or no effect on ROM score–alternate geometries were either invalid or had a near-equivalent ROM score. For the tradespace exploration, these were held constant at their nominal values, to allow for the other parameters to be explored in more depth. To explore this tradespace, the remaining eight parameters assumed ten values between the bounds listed in Table 1, including the value of the parameter in the nominal HBA. These values can be seen in Table 6. With a set of nested loops, every combination of parameter values was tested. If a geometry was invalid, by breaching any of the geometric constraints described in Section 3, that geometry was discarded. Geometries were also tested for an additional condition necessary for reasonable fit: in the suit's neutral position, the knee point of the simulated thigh had to be in front of the hip point. Geometries that were deemed viable had structures and

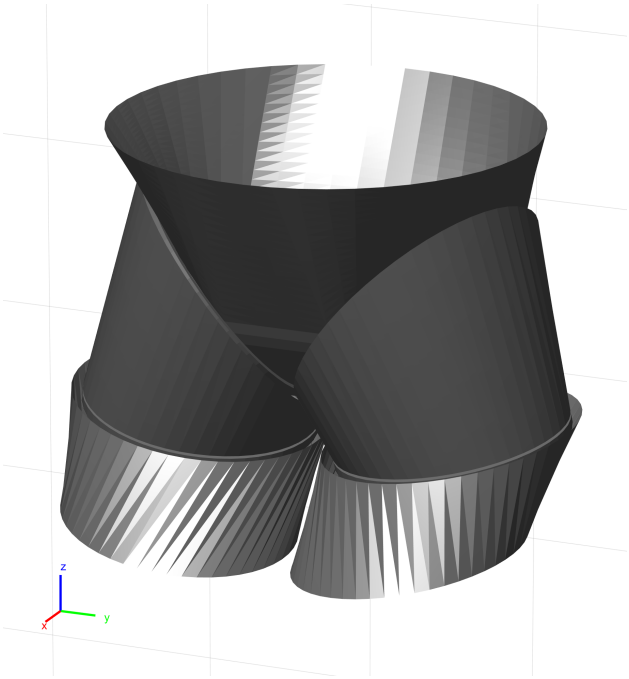


Figure 6: **Top-performing HBA geometry.**

surfaces generated according to the model in Section 2 and their ROMs scored as detailed in Section 4. This approach was implemented in MATLAB.

Several simplifications were also made. For efficiency, only the Briefs and Proximal and Distal Sections (as well as middle and upper bearings) were tested for intersection with the simulated thigh in Suited ROM estimation. The HBA components modeled were treated as symmetric across the sagittal plane. Only the left side was tested and given an ROM score. All bearings were assumed to have a thickness of one centimeter.

Of the $10^8 = 100$ million combinations of parameter values explored, 1,487,254 had a viable geometry. Of these, 52,276 geometries had an ROM score greater than or equal to the nominal HBA. For efficiency, the tradespace exploration was initially performed at low-fidelity; specifically, the edges of each component had 10 points, and the positions of the suit were checked by moving bearing angles by 15 degrees. For accuracy, all geometries which scored equal to or greater than the nominal HBA were then re-simulated at medium fidelity: the edges of each component had 20 points, and the positions of the suit were checked by moving bearing angles by 5 degrees. The 1000 top-scoring geometries in medium fidelity of these were then re-simulated once more at high fidelity: the edges of each component had 50 points, and the positions of the suit were checked by moving bearing angles by 2 degree increments. This process ensured potentially high-scoring geometries were not missed.

The HBA geometry with the highest ROM Score (measured in the high-fidelity simulation) of those explored used the parameters indicated in Table 6 and the geometry itself can be seen in Figure 6. The ROM score of this top-scoring suit geometry compared to the nominal can be seen in Table 7. The ROM of the nominal and top-scoring geometries themselves can be seen in Figure 8.

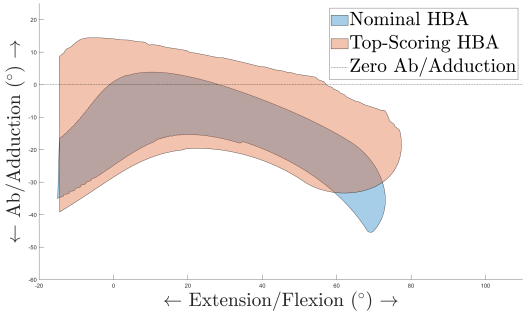


Figure 7: **ROM of top-scoring and nominal geometries in terms of ab/adduction and flexion/extension.**

As can be seen in both Table 7 and Figure 8, the top-performing HBA geometry has a much better alignment with the gait ROM than the nominal case. The top-scoring geometry permits markedly more adduction, allowing the occupant's feet to be placed closer to the sagittal plane (running through the body midline) or even in line with one another. This increased adduction, along with the greater overlap with the Unsuited ROM, should allow occupants to have a more natural gait. The top-scoring geometry also makes the Unsuited ROM extension range more accessible, due to the increased overlap. Furthermore, the ROM of the top-scoring geometry includes the leg's neutral position (straight down, indicated by the black star in Figure 8), allowing for a more natural neutral stance. Finally, as shown in Figure 7, the top-scoring geometry allows a much greater range of kneeling or squatting motions, which are important in planetary exploration. In the nominal geometry, any motion that requires flexion of more than 40 degrees requires at least 10 degrees of abduction. The top-scoring geometry can reach over 50 degrees of flexion with zero abduction.

In addition to finding new, high-scoring options for suit geometry, the large data set from the tradespace exploration permits analysis of geometric trends in the HBA. While all suits considered had two joints, it is possible to understand the effect of having only one joint by considering the geometries where the rotational axes were collinear–those that have adjacent aligned bearings. A summary of the statistics affiliated with the ROM scores for geometries with adjacent aligned bearings is shown in Table 8. It is clear these geometries score much lower than the HBA geometries overall. The maximum and mean scores of geometries with adjacent aligned bearings are less than 10% of the maximum and mean scores of the geometries as a whole. The HBAs with adjacent aligned bearings are effectively a single DoF, which creates a greater limitation on the Suited ROM. Therefore, the designs with adjacent aligned bearings would likely have significant impact on occupant mobility. This result supports previous results that locking a bearing in the HBA would drastically reduce ROM [12].

The data set was also analyzed to determine the factors that have greater influence on higher ROM score. A Partial Least Squares Regression (PLS) was applied to the data from the tradespace study. The low-fidelity data were used, to capture the entire tradespace. The predictors used were the eight parameter variables that were varied in the refined tradespace study, and the responses were the ROM scores. The number of components was set at eight, equal to the number of variables. The Variable Importance in Projection (VIP) score

Table 6: **Values explored in tradespace.**

	Values Explored									
$h_{1/2}$ (m)	-0.128[ab]									
a_1 (m)	0.032[ab]									
d_1 (m)	-0.106[ab]									
θ_1 (deg)	160[ab]									
α_1 (deg)	-52.0[ab]									
$h_{2/3}$ (m)	-0.250	-0.219	-0.188	-0.156	-0.125[b]	-0.094	-0.087[a]	-0.063	-0.031	0.00
a_2 (m)	-0.100	-0.075	-0.050	-0.025	0.00[b]	0.005[a]	0.025	0.050	0.075	0.100
d_2 (m)	-0.200	-0.175	-0.150[b]	-0.125	-0.103[a]	-0.100	-0.075	-0.050	-0.025	0.00
α_2 (deg)	-90.0	-67.5	-45.0[b]	-22.8[a]	-22.5	0.00	22.5	45.0	67.5	90.0
$h_{3/4}$ (m)	-0.250	-0.219[b]	-0.188	-0.156	-0.125	-0.100[a]	-0.094	-0.063	-0.031	0.00
a_3 (m)	-0.100	-0.075	-0.050	-0.025	0.00[a]	0.00	0.025	0.050	0.075	0.100[b]
d_3 (m)	-0.200	-0.175	-0.150	-0.125	-0.100	-0.090[a]	-0.075	-0.05	-0.025	0.00[b]
α_3 (deg)	-90.0	-67.5	-45.0	-23.1[a]	-22.5	0.00[b]	22.5	45.0	67.5	90.0

[a] Value of parameter in nominal HBA.
[b] Value of parameter in top-performing HBA.

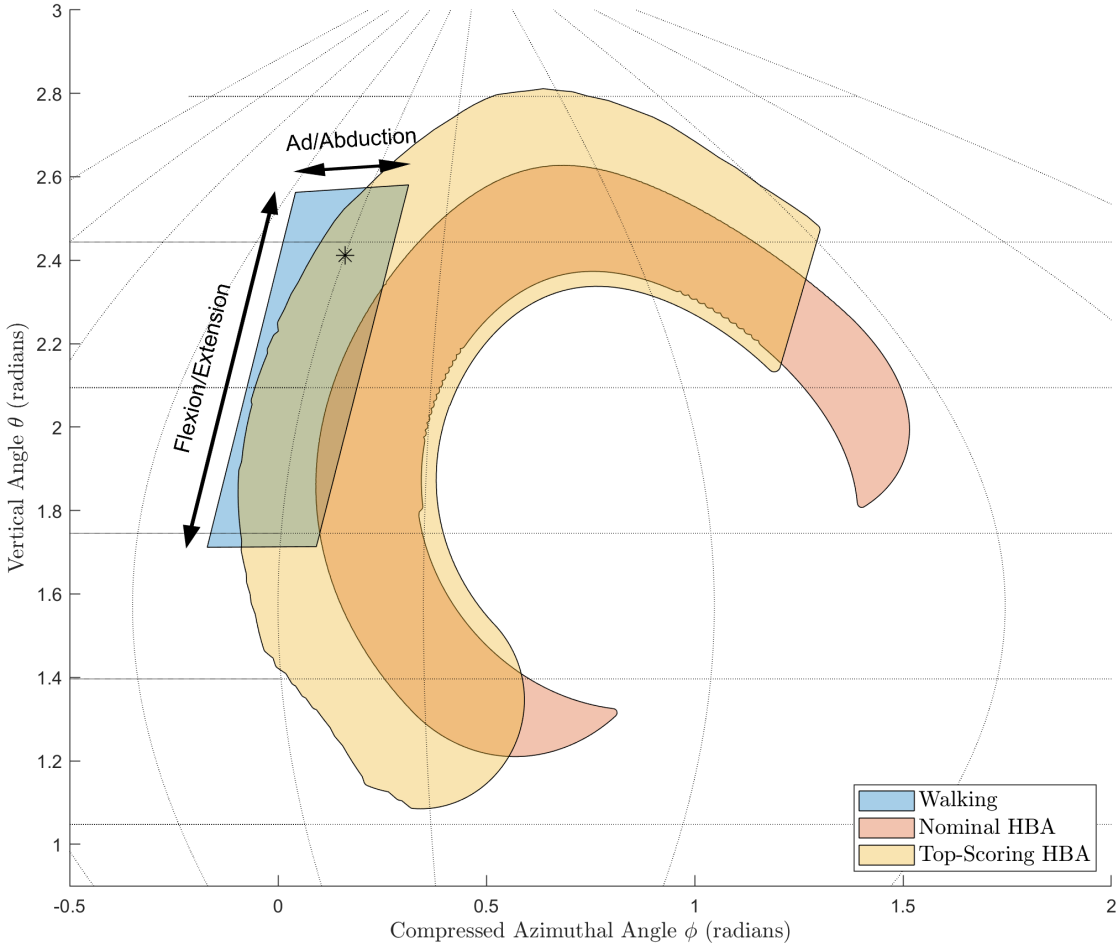


Figure 8: **Suited high-fidelity ROMs of top-scoring and nominal HBA, compared with Unsuited ROM.**

Table 7: **Summary of ROM Scores for nominal and top-scoring geometries, across various levels of modelling fidelity.**

	Nominal	Top-scoring
Low-fidelity	0.0017	0.0086
Medium-fidelity	0.0023	0.0135
High-fidelity	0.0023	0.0144
ROM Score % improvement	-	526.1%

Table 8: **ROM score statistics from HBA geometries with adjacent aligned bearings versus all geometries.**

ROM Score Stat	Set 1[a]	Set 2[b]	All
Quantity	61,722	118,028	1,487,254
Min	0	0	0
Max	0.0017	0.0018	0.0122
Mean	<0.0001	<0.0001	0.0002

[a] Set of geometries with $\alpha_2 = a_2 = 0$.
[b] Set of geometries with $\alpha_3 = a_3 = 0$.

was then determined from the loading matrices, to measure the impact of each parameter. The resulting VIP scores can be seen in Table 9.

The VIP scores of parameters α_2 and α_3 were both significantly greater than unity, indicating they were the most influential on the ROM score of a given suit geometry. Top-scoring suits (such as the one in Figure 6) have a Proximal Section which is canted outward from the sagittal plane, and a Distal Section which is canted back towards the sagittal plane. When both angles are large, there is an "out-in" geometry which could be a key factor in the higher scores. The larger angles of the components allow for more of the unit sphere to be accessed, and the magnitude of the angles appears to allow greater adduction, a key factor in high ROM scores, given the location of the Unsuited ROM.

6. ANTHROPOMETRIC ANALYSIS

The tradespace analysis in Section 5 suggested novel geometries and interesting trends, but these data were generated using a specific suit scale and parameters based on the 50th percentile male anthropometry for thigh and knee circumference. For this design to be valuable, it must be applicable

Table 9: **VIP scores from PLS on HBA parameters and tradespace ROM scores.**

Parameter	VIP Score
$h_{2/3}$	0.6479
a_2	0.1173
d_2	0.5790
α_2	2.0748
$h_{3/4}$	1.0127
a_3	0.1672
d_3	0.3192
α_3	1.3308

Table 10: **ANSUR measurements used to test geometry over varying anthropometry.**

		Values by ANSUR Number			
Sex	**Percentile**	**78** (m)	**60** (m)	**50** (m)	**D29** (m)
Female	5	0.5270	0.3470	0.3110	0.3400
	25	0.5790	0.3770	0.3360	0.3630
	50	0.6130	0.3980	0.3530	0.3790
	75	0.6510	0.4220	0.3700	0.3950
	95	0.7110	0.4650	0.4000	0.4180
Male	5	0.5320	0.3590	0.3080	0.3640
	25	0.5860	0.3870	0.3290	0.3900
	50	0.6240	0.4080	0.3440	0.4080
	75	0.6620	0.4290	0.3610	0.4270
	95	0.7230	0.4630	0.3870	0.4580

across a wide range of anthropometries. To understand the design's practicality for astronauts of different sizes, the top-scoring suit geometry was tested over a variety of different anthropometries and suit scalings. To accomplish these tests, the ROM-scoring algorithm from Section 4 was adapted.

Configurations

Each configuration tested was defined by five variables. Four of these were based in anthropometry: Thigh Radius, Knee Radius, Thigh Length, and Hip Center. However, the fifth variable was a scaling parameter for the suit dimensions, as the unscaled top-scoring geometry might not fit a very small or very large astronaut, while a linear scaling of the design might provide an improved fit by this metric.

The anthropometric variables were based on measurements from ANSUR II [22]. Four sets of ANSUR measurements were used:

- Thigh Circumference, based on ANSUR measurement #78 (Thigh Circumference), used to calculate the Thigh Radius and Hip Center values;
- Knee Circumference, based on ANSUR measurement #60 (Lower Thigh Circumference), used to calculate the Knee Radius value;
- Hip Breadth, based on ANSUR measurement #50 (Hip Breadth), used to calculate the Hip Center value; and
- Thigh Length, based on ANSUR derived measurement #D29 (Thigh Link), used as the Thigh Length value.

For each measurement, the 5th, 25th, 50th, 75th, and 95th percentiles were considered, for both males and females, resulting in two groups of five values in each set (Table 10).

Thigh Length was directly defined through the ANSUR database. Thigh and Knee Radii were calculated using the same formulas in Table 5. The Hip Center was estimated as

$$\text{Hip Center} = \frac{1}{2}(\text{Hip Breadth}) - (\text{Thigh Radius}). \quad (15)$$

To consider how the geometry might be adjusted for astronauts of different sizes, scaled versions of the top-scoring geometry were tested. The exact scalings that should be used could be considered as part of an analysis in fleet-sizing (see Section 7). This work, however, is concerned with whether such geometries could work, as opposed to the ideal scaling. As such, nine specific scaling factors were considered: 0.85, 0.9, 0.95, 0.98, 1, 1.02, 1.05, 1.1, and 1.15. In each configuration, all linear dimensions of the suit

geometry (including radii, bearing thicknesses, a, h, and d) were scaled by this value.

Every combination of these factors was considered, with $2\,(\text{sex}) \times 9\,(\text{scaling factor}) \times 5^4\,(\text{anthropometric factors}) = 11,250$ configurations total. The top-scoring and nominal suit geometries were tested for all configurations, using the medium-fidelity method described in Section 5.

After all configurations were considered, each set of sex, anthropometry, and geometry was assigned an overall ROM score equal to the highest ROM score of that set across all scalings. This was used to consider the best-case for each set, and to approximate a well-fitted suit for the given anthropometry, sex, and geometry.

Modifications for Varying Anthropometry

Every configuration was tested using the ROM-scoring algorithm in Section 4. To accommodate the varying anthropometries, two modifications were made. In particular, the knee and hip points used to define the simulated leg were adjusted based on the anthropometry of each configuration (instead of statically defined points).

The hip point of the simulated leg was assumed to fall in the same xz-plane as the hip point in the original algorithm, based on the location of the upper bearing. However, the position of the hip point along the y-axis was adjusted based on the anthropometry in each configuration. By assuming the suit's occupant was centered in the suit, the y-coordinate of the hip point was set as the Hip Center value. In other words, the hip point (in the Briefs frame) can be found as

$$ {}^1\vec{p}_h = \begin{bmatrix} 1 & 0 & 0 & 0 \\ 0 & 0 & 0 & 0 \\ 0 & 0 & 1 & 0 \\ 0 & 0 & 0 & 1 \end{bmatrix} {}^1T_2 \begin{bmatrix} 0 \\ 0 \\ h_{1/2} \\ 1 \end{bmatrix} + (\text{Hip Center})\ {}^1\hat{y}_1. \quad (16) $$

Note that this formula is places the hip point a distance of Hip Center (calculated in Eq. (15)) from the sagittal plane, but keeps the x and z positions equivalent to those as used in Section 4.

The location of the tip of the simulated leg, the knee point, was also calculated differently. In the original algorithm, it was a specific distance along the z-axis of the fourth (Distal) frame, based on the nominal Mark III HBA geometry. While computationally efficient, this meant the length between hip point and knee point changed between suit geometries. To modify this calculation for a specified Thigh Length, the knee point is re-calculated for each position. This point is chosen as the point along the z-axis of the Distal frame that lies a distance from the hip point equal to the Thigh Length. Mathematically, the knee point falls at the point ${}^3\vec{p}_k(\gamma) = {}^3T_4\,[0 \quad 0 \quad -\gamma \quad 1]^T$ (in the Distal Section Frame), where the γ variable can be found by setting Thigh Length equal to the distance between the points, expressed as $\left\| {}^1\vec{p}_k(\gamma) - {}^1\vec{p}_h \right\|$ so that

$$ \text{Thigh Length} = \left\| {}^1T_2 J(\phi_2)\, {}^2T_3 J(\phi_3)\, {}^3\vec{p}_k(\gamma) - {}^1\vec{p}_h \right\|. \quad (17) $$

By noting

$$ {}^1T_2 J(\phi_2)\, {}^2T_3 J(\phi_3)\, {}^3T_4 = \begin{bmatrix} {}^1\hat{x}_4 & {}^1\hat{y}_4 & {}^1\hat{z}_4 & {}^1\vec{q}_4 \\ 0 & 0 & 0 & 1 \end{bmatrix}, \quad (18) $$

so that ${}^1\vec{p}_k(\gamma) = {}^1\vec{q}_4 - \gamma\, {}^1\hat{z}_4$, we can solve Eq. (17) by

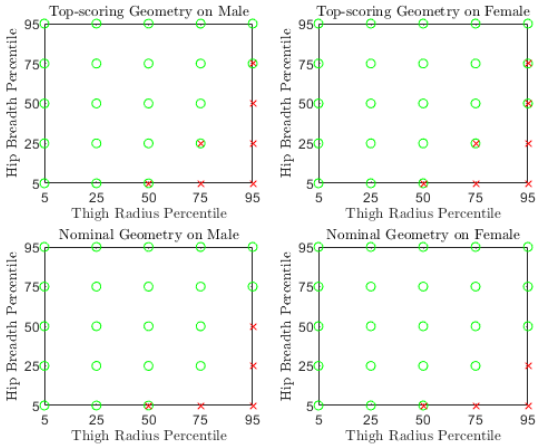


Figure 9: **Anthropometries with ROM scores less than 0.002, by sex and geometry. Green circles show anthropometries with ROM scores greater than or equal to 0.002, red crosses show anthropometries with ROM scores less than 0.002. Some points have both, indicating for that combination of Thigh Radius and Hip Breadth, some anthropometries fit and some failed.**

rewriting it as

$$ (\text{Thigh Length})^2 = \left\| \delta\vec{p} - \gamma\, {}^1\hat{z}_4 \right\|^2 \quad (19) $$

where $\delta\vec{p} = {}^1\vec{q}_4 - \left({}^1\vec{p}_h\right)_{1:3}$. Eq. (19) can be simplified to an easily solvable quadratic:

$$ (\delta\vec{p} \cdot \delta\vec{p}) - 2\gamma(\delta\vec{p} \cdot {}^1\hat{z}_4) + \gamma^2 = (\text{Thigh Length})^2. \quad (20) $$

This solution was used in the modified ROM-scoring algorithm to enable a specified fixed length.

Results for Varying Anthropometry

Assuming a minimal ROM score of 0.002 (roughly the nominal suit's ROM score for the 50th percentile male parameters) for a geometry to fit an anthropometry, the top-scoring suit design fit 1,030 of the 1,250 anthropometric configurations ($5^4 = 625$, for each sex), while the nominal geometry fit 1,042. Across both geometries and sexes, the anthropometries which failed were largely those which had a large Thigh Radius and a small Hip Breadth, as can be seen in Figure 9.

While the nominal geometry fit more anthropometries, the top-scoring geometry outscored it in most cases. Across all anthropometric and sex-based configurations, the top-scoring geometry had the greater score in 1,116 of the 1,250 configurations (Figure 10). Figure 10 also shows that there is a maximum ROM score of 0.178, which occurs when the Suited ROM area entirely contains the Unsuited ROM area, making the ROM score equal to the Unsuited ROM area, scaled by $\frac{1}{4\pi}$.

These tests indicated the top-scoring geometry (Figure 6) remains robust over varying anthropometry. However, the linear scalings used may not be appropriate or realistic for all anthropometric combinations.

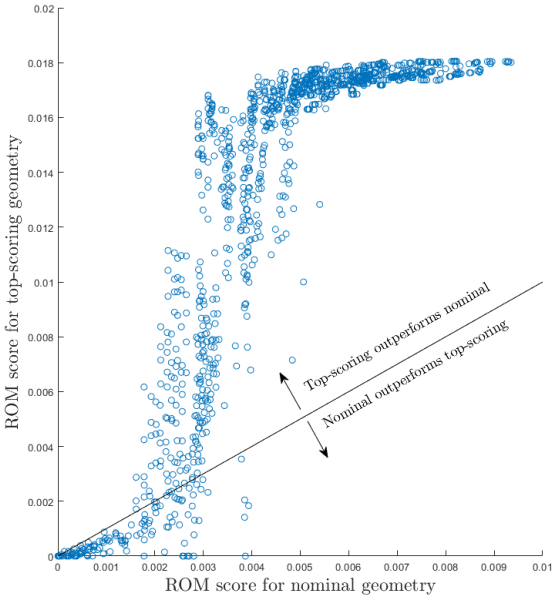


Figure 10: **ROM scores for nominal and top-scoring geometries for each anthropometry configuration. Black line shows equal scores.**

7. Limitations and Future Work

The approach and results in this paper were limited by, among other things, computational complexity. Simplifications were made (such as those listed in Section 2) and some effects were not considered. For example, the simulated thigh used to calculate the HBA's Suited ROM assumed constant positions of the knee and hip, causing the length of the thigh to vary based on suit geometry and knee position.[5] Similarly, the rolling convolute of the HBA (a joint affixed to the lower bearing that allows for small amounts of hip ab/adduction) was not modeled. In the physical suit, this joint (and the motion of the occupant relative to the suit) would allow for a range of occupant leg positions per pose, not just one. There is also an opportunity to adapt the definition of fit and ROM scoring to determine new geometries.

Future work should address these and other simplifications. As an example, when considering the different anthropometries, the method was adapted to force a fixed thigh length. Another opportunity is to use a more nuanced approach to leg compression (instead of applying a reducing factor to the leg radii), which could further improve estimation and be used to model human-suit interaction. Additionally, allowing component radii to vary and considering the motion of the rolling convolute and the suit occupant could allow for more accurate estimation. The model itself could also be extended, by parameterizing the overlap of the different components and modelling components with non-zero thickness, including the structure of the suit necessary to support the bearings or fulfill other suit requirements (e.g., pressure, thermal, or safety). Similarly, the ROM calculation could be expanded by considering the motion paths within the ROMs, not just discrete unit vectors.

[5]This variation was addressed in the anthropometric analysis in Section 6, but was too inefficient to use in the main tradespace.

The work in this paper could also be applied to other problems. In particular, re-running the tradespace analysis using variations in scale and anthropometry could be used to find a geometry that scores well over different body types, rather than identifying a geometry and then testing it for different occupants. While scalings other than linear may show better results, linear scaling could still be used for this analysis, as the non-linear variations between parameters could be contained in the various entries in the parameter tradespace. Additionally, applying this model on such anthropometric variations could be a useful tool for fleet sizing of space suit components, and could even be part of a more-complex tradespace analysis. The model and ROM scoring method can also be applied to joints other than the hip and HCJAs other than the HBA. Space suits with HCJAs at locations other than the hips (including suits with rigid components over the entire body) have been considered in the past [9], and this work could be extended to understand their impact on mobility. Mobility is not the only factor that should be considered, however. One especially useful extension or modification of this work would be one that considers other suit metrics such as mass and cost. These could be combined into a more complex objective function and the tradespace could be re-explored.

8. Summary

Soft-component space suits (such as the Apollo space suit) are susceptible to springback forces caused by changes in volume. An alternative is using hard-component joints assemblies (HCJAs), like those used in the Hip Bearing Assembly (HBA) of the Mark III suit. However, the rigid components in HCJAs act as bounds on motion, which can restrict the mobility of the suit's occupant. This research developed a way to describe and study HCJAs and their effect on the occupant's range of motion.

A method of modeling the geometry of HCJAs was developed in Section 2 based on Denavit-Hartenberg parameters, with parameters added to account for the size and placement of component edges and bearings. This model allows for description and parameterization of HCJAs, resulting in easier design iteration and simulation. In Section 3, this model was applied to the HBA, and the parameters were used to develop design constraints and parameter bounds. A system to find and describe the range of motion (ROM) of an HCJA occupant's joint was described in Section 4, as well as a method of comparing it to the occupant's unencumbered mobility. The approach considered human-suit interaction as well as the different kinematic arrangements of the suit. This method allows for rapid and efficient estimation of the impact potential suit designs may have on the occupant range of motion.

The model, constraints, and ROM scoring method were combined and used to explore possible alternate geometries of the HBA, as described in Section 5. Many geometries scored above the nominal HBA, indicating the geometry could be redesigned to allow for more mobility in terms of gait. Among these, the top-scoring geometry was highlighted, with its ROM compared to that of the nominal HBA, as well as to the ROM necessary for gait. The proposed design increased the ability to kneel by increasing the flexion that could occur without abduction. The tradespace data set also indicated one-joint suits would severely limit hip mobility and the angles of the Proximal and Distal Sections were the driving geometric factor behind larger ranges of motion. The high-

scoring geometry was shown to peform well across varying anthropometries, as shown in Section 6.

ACKNOWLEDGMENTS

This research was funded by NASA Award NNX15AR20G. Views expressed in paper are are not endorsed by sponsor.

REFERENCES

[1] S. J. Hoffman, "Advanced EVA capabilities: A study for nasa's revolutionary aerospace systems concept program," NASA Johnson Space Center, NASA Johnson Space Center, Houston, Texas, Technical Report 20040200983, April 2004. [Online]. Available: https://ntrs.nasa.gov/archive/nasa/casi.ntrs.nasa.gov/20040200983.pdf

[2] D. Newman, P. B. Schmidt, D. B. Rahn, N. Badler, and D. Metaxas, "Modeling the extravehicular mobility unit (EMU) space suit: Physiological implications for extravehicular activity (EVA)," in *30th International Conference on Environmental Systems*, 07 2000, doi:10.4271/2000-01-2257.

[3] P. B. Schmidt, D. J. Newman, and E. Hodgson, "Modeling space suit mobility: Applications to design and operations," in *31st International Conference on Environmental Systems*, Jul 2001, doi:10.4271/2001-01-2162.

[4] S. P. Chappell, J. R. Norcross, A. F. J. Abercromby, O. S. Bekdash, E. A. Benson, S. L. Jarvis, J. Conkin, M. L. Gernhardt, N. House, J. Jadwick, J. A. Jones, L. R. Lee, R. A. Scheuring, and J. A. Tuxhorn, *Evidence Report: Risk of Injury and Compromised Performance due to EVA Operations*. National Aeronautics and Space Administration, Jan 2017. [Online]. Available: https://ntrs.nasa.gov/archive/nasa/casi.ntrs.nasa.gov/20170002574.pdf

[5] C. Chullen, J. McMann, K. Thomas, J. Kosmo, C. Lewis, R. Wright, R. Bitterly, and V. Oliva, "U.S. spacesuit legacy: Maintaining it for the future," in *43rd International Conference on Environmental Systems*. American Institute of Aeronautics and Astronautics, Jul 2013. [Online]. Available: http://arc.aiaa.org/doi/10.2514/6.2013-3498

[6] R. A. Scheuring, J. A. Jones, J. D. Novak, J. D. Polk, D. B. Gillis, J. Schmid, J. M. Duncan, and J. R. Davis, "The apollo medical operations project: Recommendations to improve crew health and performance for future exploration missions and lunar surface operations," *Acta Astronautica*, vol. 63, no. 710, p. 980987, Oct 2008. [Online]. Available: https://ntrs.nasa.gov/archive/nasa/casi.ntrs.nasa.gov/20070030109.pdf

[7] D. Graziosi and J. G. Ferl, "Performance evaluations of an advanced space suit design for international space station and planetary applications," in *29th International Conference on Environmental Systems*, Jul 1999. [Online]. Available: https://www.sae.org/content/1999-01-1967/

[8] L. A. Wickman and B. Luna, "Locomotion while load-carrying in reduced gravities," *Aviation, space, and environmental medicine*, vol. 67, pp. 940–6, Nov 1996.

[9] C. W. Flugel, J. J. Kosmo, and J. R. Rayfield, "Development of a zero–prebreathe spacesuit," in *14th Intersociety Conference on Environmental Systems*, Jul 1984, pp. 840–981. [Online]. Available: https://www.sae.org/content/840981/

[10] J. J. Kosmo, W. E. Spenny, R. Gray, and P. Spampinato, "Development of the NASA ZPS Mark III 57.2-kN/m^2 (8.3 psi) space suit," in *18th Intersociety Conference on Environmental Systems*. SAE International, Jul. 1988, pp. 630–650. [Online]. Available: http://www.jstor.org/stable/44470364

[11] J. R. Norcross, K. G. Clow, L. C. Stroud, L. Desantis, J. R. Vos, and M. L. Gernhardt, "Metabolic costs and biomechanics of inclined ambulation and exploration tasks in a planetary suit," National Aeronautics and Space Administration, NASA Center for AeroSpace Information , Hanover, Maryland, Tech. Rep., June 2010. [Online]. Available: https://ston.jsc.nasa.gov/collections/TRS/_techrep/TP-2010-216125.pdf

[12] M. S. Cowley, S. Margerum, L. Hharvill, and S. Rajulu, "Model for predicting the performance of planetary suit hip bearing designs," in *4th International Conference on Applied Human Factors and Ergonomics*. National Aeronautics and Space Administration, Jul 2012, available on NASA Technical Reports Server. [Online]. Available: https://ntrs.nasa.gov/archive/nasa/casi.ntrs.nasa.gov/20130000596.pdf

[13] I. Abramov, N. Moiseyev, and A. Stoklitsky, "Concept of space suit enclosure for planetary exploration," in *31st International Conference On Environmental Systems*, Jul 2001. [Online]. Available: https://www.sae.org/content/2001-01-2168/

[14] C. R. Cullinane, R. A. Rhodes, and L. A. Stirling, "Mobility and agility during locomotion in the mark iii space suit," *Aerospace Medicine and Human Performance*, vol. 88, no. 6, pp. 589–596, Jun 2017, doi:10.3357/AMHP.4650.2017.

[15] K. A. Shorter, A. Wu, and A. D. Kuo, "The high cost of swing leg circumduction during human walking," *Gait & Posture*, vol. 54, pp. 265–270, May 2017.

[16] L. Stirling, P. Arezes, and A. Anderson, "Implications of space suit injury risk for developing computational performance models," *Aerospace Medicine and Human Performance*, vol. 90, no. 6, p. 553565, Jun 2019, doi:10.3357/AMHP.5221.2019.

[17] J. J. Kosmo and A. Ross, "Space suit mobility evaluations in lunar/mars gravity environments," in *28th International Conference on Environmental Systems*, Jul 1998. [Online]. Available: https://www.sae.org/content/981627/

[18] P. McKeen, "Modeling and tradespace exploration of a space suit hip bearing assembly using multi-degree-of-freedom range of motion analysis," Master's Thesis, Massachusetts Institute of Technology, Department of Aeronautics and Astronautics, Sep. 2019.

[19] A. Roaas and G. B. J. Andersson, "Normal range of motion of the hip, knee and ankle joints in male subjects, 3040 years of age," *Acta Orthopaedica Scandinavica*, vol. 53, no. 2, pp. 205–208, 1982. [Online]. Available: https://doi.org/10.3109/17453678208992202

[20] A. Kranzl, "Normative Gait Database," Clinical Gait Analysis website. [Online]. Available: http://www.clinicalgaitanalysis.com/data/kinematics

[21] G. Wu, S. Siegler, P. Allard, C. Kirtley, A. Leardini, D. Rosenbaum, M. Whittle, D. D. DLima, L. Cristofolini, H. Witte *et al.*, "ISB recommendation on definitions of joint coordinate system of various joints for the reporting of human joint motion-Part I: Ankle, hip, and spine," *Journal of Biomechanics*, vol. 35, no. 4, p. 543548, Apr 2002.

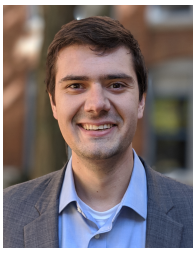
[22] C. C. Gordon, C. L. Blackwell, B. Bradtmiller, J. L. Parham, P. Barrientos, S. P. Paquette, B. D. Corner, J. M. Carson, J. C. Venezia, B. M. Rockwell *et al.*, "2012 anthropometric survey of us army personnel: Methods and summary statistics," Army Natick Soldier Research Development and Engineering Center MA, Tech. Rep., 2014. [Online]. Available: http://tools.openlab.psu.edu/publicData/ANSURII-TR15-007.pdf

[23] J. P. Snyder, *Map Projections–A Working Manual*. US Government Printing Office, 1987, vol. 1395.

[24] J. C. Seong, K. A. Mulcahy, and E. L. Usery, "The sinusoidal projection: A new importance in relation to global image data," *The Professional Geographer*, vol. 54, no. 2, pp. 218–225, 2002. [Online]. Available: https://www.tandfonline.com/doi/abs/10.1111/0033-0124.00327

[25] Mathworks, "evalclusters," Jul 2019, https://www.mathworks.com/help/stats/evalclusters.html.

BIOGRAPHY



Patrick McKeen *received a B.S. in engineering from Harvey Mudd College, Claremont, CA, USA, in 2017 and an S.M. in aeronautical and astronautical engineering from the Massachusetts Institute of Technology (MIT), Cambridge, MA, USA, in 2019. He is currently a Ph.D. Candidate at MIT in the Department of Aeronautics and Astronautics. His research focuses on space systems, cubesats and smallsats, near-future satellite technologies, and in-space manufacturing.*



Leia Stirling *received the B.S. and M.S. degrees, from the University of Illinois at Urbana-Champaign, Champaign, IL, USA, in 2003 and 2005, respectively, and the Ph.D. degree from the Massachusetts Institute of Technology, Cambridge, MA, USA, in 2008, all in aeronautical and astronautical engineering. She is currently an Associate Professor at the University of Michigan in the Department of Industrial and Operations Engineering. Her research quantifies human performance and human-machine fluency in operational settings to assess human performance augmentation, advance exoskeleton control algorithms, mitigate injury risk, and provide relevant feedback to experts across many domains, including clinical, space, and military applications.*